Flame-Spreading and Combustion in Packed Beds of Propellant Grains

Herman Krier,* S. Rajan,† and W. F. Van Tassell‡
University of Illinois at Urbana-Champaign, Urbana, Ill.

This paper is concerned with the prediction of the pressure history during the process of flame-spreading and combustion of solid-propellant grains as would occur, for example in a gun cartridge. Solution of the governing conservation equations for the two-phase media requires the use of empirical relations to account for the physical processes of momentum and energy interaction between the solid grains and hot propellant gas. The results indicate the extreme importance of these interaction relations on the predictions of the pressure and velocity field.

Nomenclature

A,B = burning rate constants, $\dot{r}=A+BP^n$
C_v,C_p = specific heat, Btu/lbm-°R
D_p = particle diameter, in.
$\mathfrak{D}$ = drag interaction term, lbf/ft^3
E = total energy, Btu/lbm [see Eqs. (10) and (11)]
E_{chem} = total propellant energy release, Btu/lbm
G_{12} = modified Nusselt number (heat-transfer coefficient), sec^{-1}
k = thermal conductivity, Btu/ft-sec-°R
L,L^* = bed length, in.
n = burning rate index
P = pressure
$\dot{r}$ = propellant regression rate
T = temperature, °R
t = time, sec
U = velocity
V_P = propellant grain volume
x = coordinate along propellant bed
Γ = mass source term, lbm/sec-ft^3 [see Eq. (15)]
ρ = density, lbm/ft^3
ϕ = void fraction = gas volume/total volume
ψ = primer mass discharge per unit length, lbm/sec-in.

Subscripts

g = gas phase
p = propellant (solid) phase
m = mixture
0 = initial (ambient)
12 = from solid to gas
21 = from gas to solid

I. Introduction

THIS paper is an analysis of flame-spreading and combustion of small solid-propellant grains in gun cartridges, applying a two-phase continuum model previously developed in Ref. 1. The physical problem may be described as a solid-propellant combustion process which is sustained by convection of heat into the unignited propellant bed base type and is contained in a cylindrical chamber which is filled completely. At one end of this chamber is the igniter assembly, and at the other is a projectile which will begin to move at a given prescribed pressure. This "piston" then moves through a long length of channel of the same cross section as the chamber, in order that the flow processes following piston motion can be followed. A predescribed igniter mass flow provides gaseous products which, in turn, ignite the bed. Since solid propellants have high burning rates, the rate of gas generation within the chamber is high. Therefore, the pressure is rising rapidly during this flame-spreading process. The pressure rises enhances the pressure-dependent burning rate of the propellant, the result of which is a rapidly accelerating combustion process, with generally steep gradients along the length of the chamber. This gradient results in a high-velocity flow of the gases toward the piston end and into the unburned portion of the propellant. Hence, the flame-spreading and pressurization is rapid, and the entire burn is completed in a matter of milliseconds, if the ignition source is strong enough.

Looking at flow process taking place, one may determine the effect on the particle bed. The hot igniter gases initially are driven into a quiescent bed of propellant particles. These ignite the particles nearest the igniter source. The mass generation and subsequent pressurization occur, and a flowfield develops within the chamber. The propellant particles exert a drag force on the flowing gases and are accelerated. As shot-start pressure is approached, the entire bed usually has been set into motion.[1] Throughout the burn, the particles continue to decrease in size as they burn. Kuo and Summerfield[2] have pioneered the analysis of packed-bed solid-propellant combustion.

II. Concept: The Continuum Model

Details of the formulation of the model are given in Ref. 1. In creating an analytical model for such a flow problem there are three possible approaches (as discussed in Ref. 1). One approach is to do a statistical analysis of the problem, following each propellant particle separately, similar to the kinetic theory of gases. Whereas this seems like an ideal approach, it is highly impractical. Another method is to use an averaging technique for the various flow properties. This approach has been utilized with some success by Gough.[3] The third approach is the continuum mechanics technique, in which the model is constructed to follow the rigid continuum mechanics principles. In this approach the gas and solid are considered as separate continua that interact with each other. This is the approach adopted in Ref. 1 and is based on the basic theory of Truesdell and Toupin.[4] The assumption upon which the continuum model is based may be listed as follows:

1) All species are present simultaneously at all points in space.

2) The mixture properties are a mathematical consequence of the species properties.

3) Each species may be considered isolated from the mixture when its motion is calculated, provided that the in-

Presented as Paper 75-240 at the AIAA 13th Aerospace Science Meeting, Pasadena, Calif., Jan 20-22, 1975; submitted Jan. 29, 1975; revision received April 3, 1975. This research was supported by the U.S. Army Ballistic Research Laboratories under Contract DAAD 05-72-C-0415.

Index categories: Multiphase Flows; Reactive Flows.

*Associate Professor, Department of Aeronautical and Astronautical Engineering. Member AIAA.

†Research Associate, Department of Aeronautical and Astronautical Engineering. Member AIAA.

‡Presently Senior Engineer, Bell Aerospace Company, New Orleans Operations. Member AIAA.

teractions between the various species are accounted for appropriately.

4) The mixture is a homogeneous substance and obeys the usual conservation laws.

5) The mixture is a Newtonian fluid.

6) The mixture pressure is the sum of the species partial pressure. Using these underlying assumptions, the one-dimensional equations have been derived earlier[1] and are listed below.

Mass Balances

$$\text{Gas Phase:}\quad (\partial/\partial t)\ (\phi\rho_g) + (\partial/\partial x)\ (\phi\rho_g U_g) = \Gamma_g \tag{1}$$

$$\text{Solid Phase:}\quad (\partial/\partial t)\ [(1-\phi)\rho_p] + (\partial/\partial x)\ [(1-\phi)\rho_p U_p] = \Gamma_p \tag{2}$$

Momentum Balances

$$\text{Gas Phase:}\quad \rho_g\phi(DU_g/Dt_g) = -(\partial/\partial x)\ (\phi p_g) + (\partial/\partial x)\ [(U_g-U_m)^2\rho_g\phi] - (U_g-U_m)\Gamma_g + \mathfrak{D} \tag{3}$$

§

$$\text{Solid Phase:}\quad (1-\phi)\rho_p(DU_p/Dt_p) = (\partial/\partial x)\ [(1-\phi)\rho_p(U_p-U_m)^2] - (U_p-U_m)\Gamma_p - \mathfrak{D}[(1-\phi)/\phi] \tag{4}$$

Energy Balances

$$\text{Gas Phase:}\quad \phi\rho_g(DE_g/Dt_g) = (\partial/\partial x)\{U_g[-\phi P_g + \rho_g\phi(U_g-U_m)^2]\} + \Gamma_g(E^g_{\text{chem}} - E_g) + (\partial/\partial x) \times [\phi\rho_g(U_g-U_m)E_g] - (\partial/\partial x)\ \{(U_g-U_m)\ [-\phi P_g + \phi\rho_g(U_g-U_m)^2]\} + C_g\phi G_{12}(T_p-T_g)\rho_g \tag{5}$$

$$\text{Solid Phase:}\quad (1-\phi)\rho_p(DE_p/Dt_p) = (\partial/\partial x)\{U_p \times [(1-\phi)\rho_p(U_p-U_m)^2]\} + \Gamma_p(E^p_{\text{chem}} - E_p) + (\partial/\partial x) \times [(1-\phi)\rho_p(U_p-U_m)E_p] - (\partial/\partial x)\ \{(U_p-U_m) \times [(1-\phi)\rho_p(U_p-U_m)^2]\} + C_p(1-\phi)\rho_p G_{21}(T_g-T_p) \tag{6}$$

An appropriate form of the boundary conditions again is presented in Ref. 1; the following auxiliary relations also are included:

$$P_g = \rho_g \bar{R}_g T_g \tag{7}$$

$$P_p = 0 \tag{8}$$

$$\rho_p = \text{const} \tag{9}$$

$$E_g = C_{v_g}(T_g - T_0) + \tfrac{1}{2}U_g^2 \tag{10}$$

$$E_p = C_{v_p}(T_p - T_0) + \tfrac{1}{2}U_p^2 \tag{11}$$

$$\rho_m = \rho_{\text{gas}} + \rho_{\text{solid}} \tag{12}$$

or

$$\rho_m = \phi\rho_g + (1-\phi)\rho_p \tag{13}$$

and

$$\rho_m U_m = \phi\rho_g U_g + (1-\phi)\rho_p U_p \tag{14}$$

§$D/Dt \equiv (\partial/\partial t) + U_g(\partial/\partial x) - D/Dt = (\partial/\partial t) + U_p(\partial/\partial x)$. Also see Appendices A and B for some additional discussion as it concerns these balance equations.

The subscript p denotes propellant, the subscript g denotes gas, and the subscript m indicates the mixture. The bed porosity ϕ is the ratio of void gas to total control volume. Hence, the ratio of solid-propellant volume to total control volume is $1-\phi$.

The solution of the continuum model requires a knowledge of all of the source terms present. The analysis also requires 1) propellant ignition model [specifying a T bulk (ignition)], 2) burning rate model [Γ_g (or Γ_p)], 3) propellant energy release [E^i_{chem}], 4 primer model [igniter mass flux history], 5) drag correlation $\mathfrak{D}$, and 6) heat-transfer correlation [G_{21} (or G_{12})]. The final forms will be discussed briefly.

For ignition, the model assumes that the bulk propellant temperature must be greater than some critical temperature, say 570°R. The question of how to model the propellant ignition properly is not discussed in this paper; however, the concept of a critical ignition temperature is exactly the same as specifying a critical *energy* having been deposited to the solid phase. The 570°R ignition temperature corresponds to a 30°R rise over the initial bulk temperature. Although quite simple, this ignition model has proved sufficient[1] in the flame-spreading rates predicted and seems very reasonable.

The burning rate law is a simple pressure-dependent law:

$$\dot{r} = A + BP^n$$

Therefore,

$$\Gamma_g = (1-\phi)\rho_p\dot{r}(S/V)_p \tag{15}$$

where $(S/V)_p$ is the effective surface-to-volume ratio of each propellant grain. In actuality, the model should use a dynamic burning rate, wherein the heat transfers to the samples.

The primer model is the same as that used by Gough[3] and is reviewed in Ref. 1. For the one-dimensional case the primer is assumed to be a source of heat and mass, distributed over a short portion of the charge. The primer provides these hot gases, which are assumed to be identical to the other gases pressent, for a finite period of time, ranging for 1-3 msec. Because of the one-dimensionality of the equations, the primer gases are assumed to mix instantaneously in the radial direction. This assumption becomes realistic only for short primer lengths with respect to the propellant bed length.

The interaction of the two continua, sources 5 and 6, is of utmost importance to this model as noted in assumption 3. The two basic interaction processes involved in the problem are the drag force between the gas and the particles, $\mathfrak{D}$, and the heat transfer from the gas to the propellant, G. These interactions must be represented by empirical correlations. However, to date, no correlations for flows of exactly this type have been found in the literature. The problem is somewhat similar to flow in porous media and, in particular fluidized systems. It is hoped that results from this field can be applied to the preceding problem.

The boundary conditions applied to solve this problem are obtained by utilizing conservation of mass, momentum, and energy at both walls, as discussed briefly in Sec. IV. It is assumed that both the gas and particle velocities are, at all times, equal to the wall velocities. In addition, an adiabatic wall condition is assumed. The propellant density ρ_p is assumed constant.

III. Fluidization Interaction

The drag interaction [the term $\mathfrak{D}$ in Eqs. (3) and (4)] and the heat-transfer coefficient [the term G in Eqs. (5) and (6)] are inputs to the model; one searches the literature for experiments which provide data to express those relations. However, tests for the operating conditions of a fluidized system have not approached the high pressures, temperatures, and velocities found in burning propellants in cartridges. Measurements on fluidized systems never have been made on accelerating flows and only on one particular phase, but the

propellant is accelerating constantly and includes all of the different regimes. Another difference is in the flow at the boundaries. Whereas the gas flows completely through a fluidized system, there is a zero-velocity boundary condition at each end of the propellant problem for the major part of the combustion process. These discrepancies in the two flows show that the flows, although appearing similar, are, in actuality, very different. However, at the present time, the fluidization field is the only source of the needed information available. Unfortunately, how much error these differences introduce into the final solution is not known.

The fact that the particles are generating gases may affect significantly both the drag and heat-transfer characteristics of the postignition bed. When particles begin to pyrolyze, the flowfield around these particles must be drastically different from the flowfield around similar, but inert, particles. The gas generation process changes the boundary layer on particles. Therefore, the rate of heat transfer to the particle must be changed since the boundary layer has an important effect on heat transfer. The same argument also may be applied to the frictional forces on the particles. The flow of gases away from the particle may be assumed to act as a buffer and to insulate the particles, thereby reducing the heat transfer and also reducing frictional forces. A constitutive statement that, once pyrolysis begins, heat transfer by convection ceases to play a role in the combustion model usually is specified.

The application of fluidization results to the granular-propellant problem actually is quite straightforward. Heat-transfer coefficient correlations for the different modes of heat transfer have been developed in the literature and are reviewed in Ref. 5. For the problem at hand, only convective heat transfer between the solid and gas will be assumed necessary. As was stated earlier, the convection rate is so large that general axial-direction heat conduction is negligible. The convective heat-transfer correlation then may be used to obtain the heat-transfer coefficient directly. The drag-interaction term is not as simple.

The major assumption needed when considering the drag is that the drag is related directly to the pressure drop across the system. Therefore, it is assumed that the pressure drop across a fluidized system is a direct consequence of the presence of the solid. In most correlations found in the literature, the pressure drop is given as a pressure difference per length of bed: a force per unit volume. Therefore, the pressure drop is related to drag by $\mathfrak{D}=\phi(\Delta P/L)$. The pressure-drop correlations then may be used in this manner as long as the transport regime is not reached. The exact details of the drag in the transport regime are discussed in Ref. 5. Table 1 shows the correlations studied in Ref. 5.

Figure 1 depicts the predictions of the pressure history in a gun cartridge 30 in. long, before shot start, showing the gross effects of the magnitude of the drag term for a typical form of the drag correlation.[5] Here $U_{\text{diff}}=U_g-U_P$ and D_p is the effective diameter of the propellant grains. It can be seen that, less drag results in greater amounts of ignition and generally higher pressures. The high-drag cases result in no ignition and

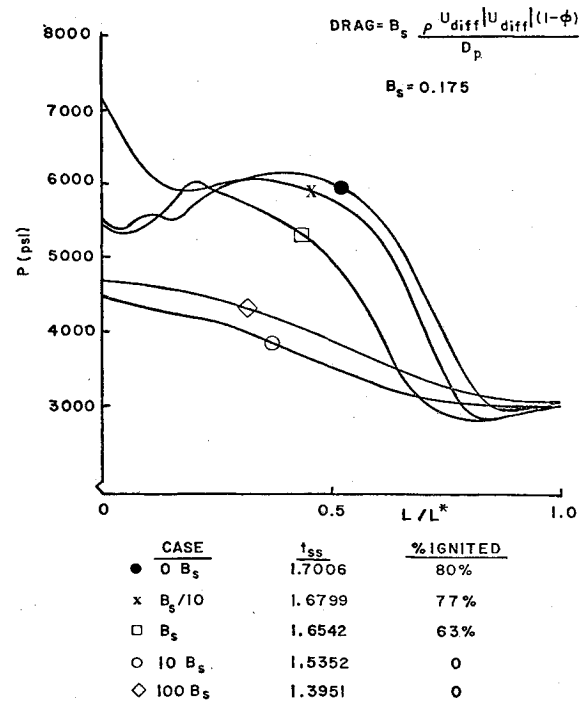

Fig. 1 Pressure distribution at shot start: effect of gas-particle drag parameters.

smooth pressure profiles because of simple pressureization by the primer. This can be explained on the basis of gas velocity. With high drag, the gas velocity will be low, and the rate of convective heat transfer will be low. It is obvious that the proper magnitude of the coefficient B_s must be used before the model can be compared with tests carried out in the gun cartridges.

Just as important is the proper input for the unsteady heat transfer from the hot ignitor and propellant gases to the solid-propellant grains. The term G_{12} in Eq. (5) is essentially the heat-transfer coefficient, and is related to the Nusselt number by

$$G_{12}=N_u k/(D_p^2 \rho_g C_g) \tag{16}$$

where k is the gas conductivity. Table 2 summarizes the correlations for the Nusselt number studied in Ref. 5. As the Reynolds number of the flow increases (because of increased pressure), the correlations presented in Table 2 show large differences from one another. The dilema exists, therefore, as to which correlation should be used to analyze the conditions found in a cartridge. A detailed analysis of effects of each of these heat-transfer correlations is given in Ref. 5. Experiments now are needed to verify whether any of these provide realistic predictions.

Table 1 Four better pressure drop correlations for backed beds

Investigator	Correlation	Particles	*Re* Range	Porosity
Ergun[9]	$\frac{\Delta P}{L} g_c = 150 \frac{(1-\phi)^2}{\phi^3} \frac{\mu U_m}{d_{p2}} + 1.75 \frac{1-\phi}{\phi^3} \frac{\rho U_m^2}{d_p}$	Smooth spheres	1-3000	0.04-0.65
Carman[10]	$\frac{\Delta P}{L} g_c = 1.5 \frac{(1-\phi)}{\phi^3} \frac{\rho U_m}{d_p} \left[1+182.4 \frac{1-\phi}{Re}\right]$	Smooth spheres	1-10,000	$\phi=0.42$
Burke and Plummer[11]	$\frac{\Delta P}{L} g_c = 3.5 \frac{\rho U_m^2}{2d_p} \frac{1-\phi}{\phi^3}$	Smooth spheres	$\frac{Re}{1-\phi} > 1000$	0.40-0.65
Leva[12]	$\frac{\Delta P}{L} g_c = 0.0365 \frac{\lambda^{1.1} \rho U_m^2}{Re^{0.1} d_p}$	Clay balls	200-15,000	0.35-0.45

Table 2 Heat-transfer correlations

Investigator	Correlation	Particles	*Pr*, *Re* range	Porosity
I. Packed Beds				
Denton[13]	$Nu=0.58\,Re^{0.7}Pr^{0.3}$ [a]	Spheres	$50\leq Re\leq 50{,}000$ $Pr<0.5$	$\phi=0.37$
Coppage and London[14]	$Nu=0.21\,Re^{0.69}Pr^{-2/3}$	Spheres	$25\leq Re\leq 550$ $Pr=0.71$	$\phi=0.38$
Gupta and Thodos[15]	$Nu=(2.06/\phi)\,Re^{0.425}Pr^{1/3}$	Spheres	$100<Re<10{,}000$	...
Bird et al.[11]	$Nu=0.555\,[Re/5.46(1-\phi)]^{0.59}Pr^{1/3}$	Spheres	$Re\geq 50$	...
II. Fluidized beds				
Gelperin & Einstein[16]	$Nu=2+0.4\,(Re/\phi)^{2/3}Pr^{1/3}$	Spheres	$Re/\phi>200$	...
Franz[17]	$Nu=0.015\,Re^{1.6}Pr^{1/3}$	Spheres	$1<Re<100$	...

[a] $Re=\rho U_0 d_p/\mu$; U_0 = superficial velocity.

IV. Numerical Computation Procedure

The two-phase porous burning problem just described is comprised of a set of six balance equations for the gas and solid phases, along with other algebraic and empirical relationships. The highly transient nature of the flame-propagation process and the existence of steep gradients in the flows variables requires the use of a numerical solution technique that provides stable and accurate solutions under a wide range of flow conditions. The numerical computational procedure must be capable of handling the oscillations resulting from the interactions of the rapid transient combustion of the porous propellant and the expansion caused by the moving projectile boundary of the charge. These demanding conditions call for the use of a numerical technique where stability can be assured by the use of an externally controllable diffusive damping parameter, since initial efforts using a straightforward two-step numerical scheme, without external damping, proved unstable. Therefore, in the present calculations a modified form of the explicit two-step Richtmyer variation of the Lax-Wendroff scheme (employed previously by one of the investigators[6] in the transonic flow calculations) has been used. Theoretically, stability is assured by observing the Courant-Friedrichs-Levy criterion, and an accuracy between first and second order in time and space is predicted. However, the dominant nature of the source terms involving high-energy release rates necessitates the use of some damping technique to obtain stable computations, since the simple Courant-Friedrichs-Levy criterion proves to be inadequate. For a simple vector equation of the form

$$(\partial F/\partial t)+A(\partial F/\partial x)=0 \tag{17}$$

where F is a given column vector and A a constant matrix of coefficients, the two-step scheme discussed in Ref. 6 introduces two additional diffusive terms of the form

$$\epsilon\frac{\Delta x^2}{2\Delta t}\frac{\partial^2 F}{\partial x^2}+\Delta t\left[A\frac{\partial^2 F}{\partial x^2}-\frac{1}{2}\frac{\partial^2 F}{\partial t^2}\right] \tag{18}$$

where Δt and Δx are the time and space increments, respectively.

The first diffusion term contains a second-order space derivative with an artificial viscosity coefficient proportional to ϵ. Thus, an explicit artificial viscosity is introduced into the computations in addition to the implicit viscosity of the numerical scheme, and can be varied by specifying the value of ϵ. For the computations reported herein, the value of ϵ used was 0.15. To test the influence of this external artificial viscosity, a computationally stable case was run with values of $\epsilon=0.05$ and 0.15, with excellent agreement of the computed results. It may, however, not be necessary to apply such artificial viscosity concepts when utilizing the explicit McCormack scheme. (See the work of Gough[3] for such an example.)

The porous propellant is contained in a chamber of specified length, the diameter of the chamber being small in relation to its length, such that the problem approximates the one-dimensional case. The charge is ignited by a primer of specified length and strength along the axis of the charge. Initially, the ends of the chamber are closed and the velocities of the gas and particles at the breech and projectile ends are equal to the atmospheric values, as also is the particle temperature. The primer then is ignited and computation of the ensuing combustion process if accomplished using a system of grid points, the number of which may be varied as computation proceeds. After a certain pressure equal to the "shot-start" pressure is reached at the projectile end of the charge, this boundary begins to move out with a velocity given by the laws of projectile motion under the influence of the pressure at the projectile base.

The values of the gas and particle velocities at the projectile base are also zero until the projectile begins to move outwards, and post-shot-start values are obtained from the laws of projectile motions. Therefore, the boundary values for the gas density, gas-phase energy, solid-phase energy, and the porosity need to be specified at the breech and projectile ends. These boundary values at the breech and projectile ends are computed from the conservation form of the governing equations. Thus, for a small volume element ΔV, with boundaries $(x\pm, y\pm)$, and a unit depth, the gas-phase mass conservation may be written in integral form as

$$\frac{\partial}{\partial t}\int_{\Delta v}(\phi\rho_g)\,dxdy+\int_{y-}^{y+}(\phi\rho_g U_g)\Big|_{x}^{x+}dy$$

$$=\int_{\Delta v}\Gamma_g\,dxdy \tag{19}$$

Similar equations may be written for the other governing equations. After further simpliciations, this equation may be written as

$$(1/\Delta t)\ [\tfrac{1}{2}\{(\phi\rho_g)_j^{n+1}+(\phi\rho_g)_{j-1}^{n+1}\}-\tfrac{1}{2}\{(\phi\rho_g)_j^{n}+(\phi\rho_g)_{j-1}^{n}\}]$$

$$=(1/\Delta x)\ [(\phi\rho_g U_g)_j^n-(\phi\rho_g U_g)_{j-1}^n]+[\Gamma_g]_{j-(1/2)}^n \tag{20}$$

with cell boundaries at $j\Delta x$ and $(j-1)\Delta x$. Here $(\phi\rho_g)_g^{-n}$ is the value of $(\phi\rho_g)$ computed at $j\Delta x$ and time $n\Delta t$. Similar equations may be written for the solid-phase mass conservation and the solid- and gas-phase energy conservation.

If the point $j\Delta x$ is considered to be at the projectile boundary, we may compute readily the boundary values at $(n+1)\Delta t$ from Eq. (20), since we have all of the values up to the boundary point computed at $(n+1)\Delta t$. For the breech-end boundary-point calculation, there are insufficient data in applying the finite-difference form of the conservation equations directly. As a first approximation, it is assumed that the values at a mirror point beyond the breech-end boundary are the same as the values at the boundary point. Based

Table 3 Code input parameters for modeling a 76-mm gun experiment[a]

Initial bed temperature T_0	540°R
Initial porosity ϕ	0.48
Propellant burning rate ($r=bP^n$) ($M6$ propellant) b	0.00553 (in×sec)/(psi)^n
n	0.667
Propellant density ρ_p	0.057 lbm/in.^{3}
Outside diameter of seven-perforated grain d_p	0.285 in.
Diameter of perforation	0.028 in.
grain length	0.662 in.
Bulk ignition temperature T_B	570°R
Molecular weight of propellant gas MW	22.93
Chemical energy (heat of combustion)	1.26×10^8 lbf-in./lbm
Covolume of propellant gas η	23 lbm/mole
Bed length L	18 in.
Primer length	10 in.
Primer on-time t_p	4.0 msec
Primer mass discharge rate ψ	1.0 lbm/sec-in.
Bed diameter	3.0 in.
Shot-start pressure	3000 lbf/in.^{2}
Projectile (total piston) weight	15.0 lbm
Drag interaction term: drag $=B_s[(1-\phi)/\phi^2](\rho_m U_m^2/dp)$	$B_s=0.175$
Heat-transfer interaction term: $G_{12}=(k/d_p)[2+0.4(R_e/\phi)^{2/3}P_r^{1/3}]$ where k = thermal conductivity $=\mu c_p/P_r$	

[a]Gun input parameters provided by McClure and East[7] and Horst.[24]

on this approximation, the values at the boundary point and the values at an interior point adjacent to the boundary first are computed. An iterative procedure then is employed, using the finite-difference form of the conservation equations to refine the approximation at the breech-end boundary to satisfy the conservation equations. Results computed in this manner for both the closed-chamber and moving-projectile boundary cases are presented in Sec. V.

V. Some Typical Results

This section presents the predictions of the pressure history and distribution in one-dimensional channels loaded with solid-propellant grains, along with the subsequent variations of gas-and-solid-particle velocities, flame-spreading rates, and unsteady value for the porosity. All of the results represent the conditions for moderately loaded ($\phi\geq0.30$), multiperforated cylindrical grains in fairly long beds.

Since the one original purpose of this work was to develop a model to predict the pressure dynamics in large cartridges and full-scale charge assemblies, the discussion of our results is centered about a comparison of the predictions of the model with those experiments reported by McClure and East.[7] Table 3 presents the pertinent parameters used as input to the model so as to simulate one series of test results with a 76mm cartridge. Figures 2-8 present these predictions.

The first unknown to be modeled in order to attempt a comparison with the tests is that of the primer tube discharge function. We have utilized the formulation as presented by Gough.[3] This model must assume instantaneous mixing lateral to the primer, since the code is a one-dimensional one. Details are not presented here, but, specifically, one must set a mass discharge of high-temperature gases along a prescribed primer length.

Figure 2 presents the pressure distribution history due to the primer discharge along in a fully loaded bed of *inert* grains having the same geometry as the actual propellant. The primer is set to be 10 in. long in an 18-in bed of inert propellant. For the length of 10 in., the average discharge was used ($\psi=1.0$ lbm/sec/in.) and lasted 4 msec to consume 0.04 lbm of primer material.

The predictions of the pressure history with the actual propellant bed for the primer function of $\psi=1.0$, $t_p=4$ msec, is shown in Fig. 3 at the $x=10$-, 6-, 12-, and 18-in. position. Note the steepening of the pressure rise as one observes the pressure interior of the bed. A pressure front can be assumed to propagate into the propellant, being driven by the combustion (flame) front at an approximate speed of 8 in./msec (667 fps). This compares with the value of 985 fps reported by McClure and East.[7] Here the pressure front propagation speed, V_{PR}, is the slope of the locus of distance vs time when the pressure begins abruptly to increase. The slow initial rise at the front (breech) end is due to the primer action, before propellant ignition is reached.

Figure 4 presents the predicted pressure distribution history at various times until the condition that pressure greater than 25,000 psi is reached somewhere in the cartridge. This upper limit on pressure was the condition for case rupture,[7] Notice the buildup of a "continental divide" at 3.4 msec at $x\simeq13.0$ in. Actually, the data provided by McClure and East do not indicate such a dramatic pressure peak; however, the distributions, as shown for time greater than 3.6 msec, are similar to those observed in the experiment. It should be noted that the model assumes an exact one-dimensional flow, that is, a constant-area tube at all times. If the fiber-glass cartridge, at any time before rupture, expanded its diameter due to the rapid pressure buildup, or if the simulated projectile moved forward in the experiment before case rupture, it is surmised that the pressure front might not be as large as predicted by the one-dimensional equations for the constant volume conditions.

The flame front locus during the pressure buildup just discussed is shown in Fig. 5. The average flame speed of 5.5 in./msec (458 fps) compares well with the observed $V_f=520$ fps during the latter part of the flame-spreading sequence. The experimentally observed speed of 1460 fps in the first half of the bed apparently can be attributed, in the main part, to the flame propagation through the primer. Additional

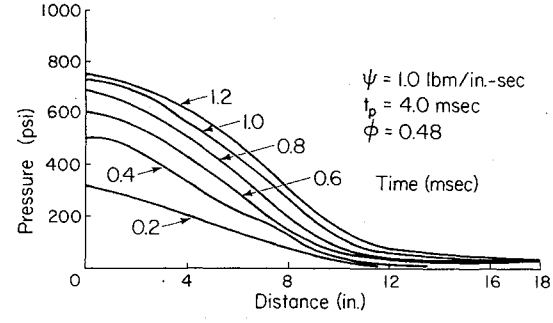

Fig. 2 Pressure distribution in an inert propellant bed showing primer response; Note; $T_{ign}=570°R$ was reached after 1.55 msec at $x=0$.

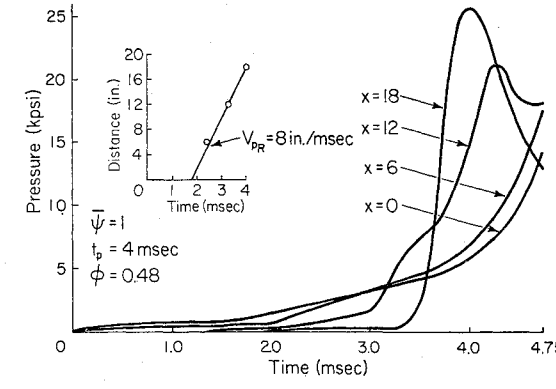

Fig. 3 Pressure history at $x=0$, 6, 12 and 18 in., predicted for conditions simulating a 76mm cartridge.

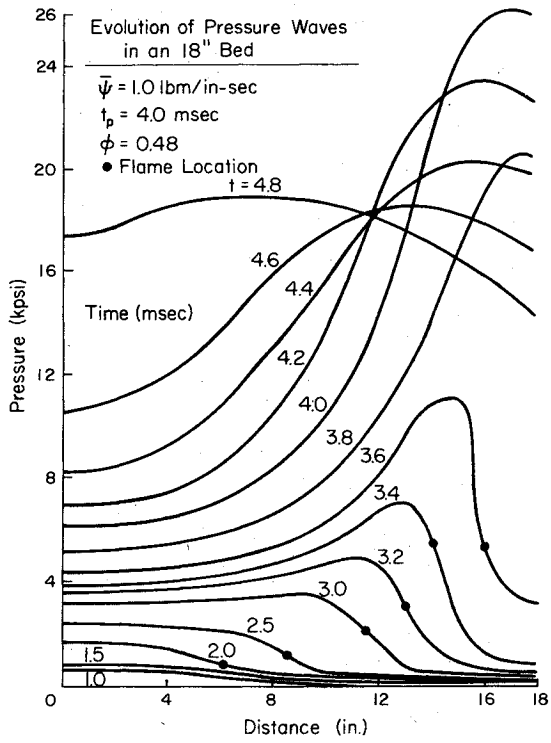

Fig. 4 Pressure distribution history predicted for conditions simulating a 75-mm cartridge ($\psi = 1.0$).

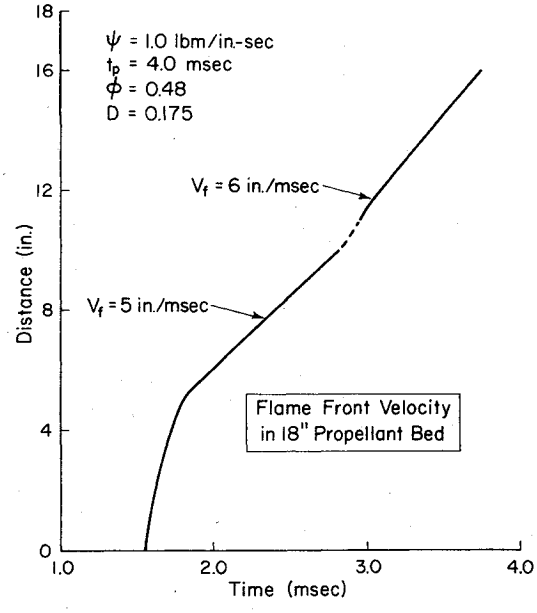

Fig. 5 Flame front location predicted for conditions simulating a 76-mm cartridge.

calculations[8] have shown that the magnitude of a predicted flame speed is a direct function of the assumed bulk ignition temperature, as well as the drag and heat-transfer interaction correlations used, implying that, in actuality the modeler needs more input data in order to fix those parameters which represent a physically real test correlation.

An insight into the behavior or the solid-propellant grains during the ignition sequence can be made by observing the predicted porosity ϕ distribution for various times, as shown in Fig. 6. Notice that the mobility of the grains and the burning away of the propellant, first at the front end ($x=0$), clearly is evident in the porosity distribution history.

Finally, for additional information into the gasdynamics of the process, predictions of both the gas velocity and particle

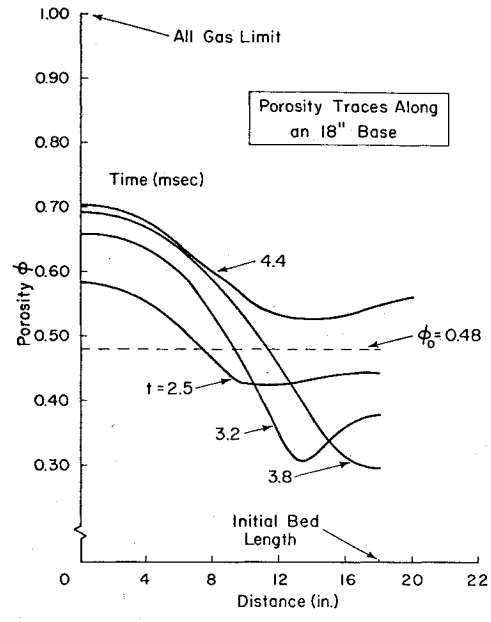

Fig. 6 Porosity distribution history predicted for conditions simulating a 76-mm cartridge.

velocity distribution are shown in Figs. 7 and 8 respectively. It is interesting to notice the lag in the grain velocity compared to that of the gas for several different times. Both velocity distributions at time $t=4.8$ msec were the continuing condition of a moving piston and hence nonzero velocities at one end. In the experiment with this particular cartridge there was some allowance for expansion of crushable spacer wads between the bed and the projectile. Comparing the reported grain velocity distribution with the predictions shown in Fig. 8, there is fairly good agreement.

The reader is referred to the work of Gough[3] which also is reported for a prediction of that model for the same 76-mm gun system. In many respects, both models agree in their predictions. There are, of course, very important differences; in particular, the predictions of the Gough model result in very uniform pressure distributions as time increases, unlike those predicted in Fig. 4.

VI. Conclusions

The objective of the modeling was to develope a predictive code for use in the analysis of the nonsteady pressure and flow field in a packed cartridge during ignition. Although the approach to the theoretical modeling of this reactive two-phase system can vary and the governing conservation equations might appear different depending on the approach,[2,3] the problem with any form of the modeling is that a great deal of empiricism still is required.

Until the empirical data base is established for this problem, it is our contention that the proper interpretation of predictions and an accurate comparison with test result cannot be made. As discussed, the required semi-empirical data needed includes 1) an ignition criterion for the propellant grains, 2) a nonsteady burning rate relation, 3) a model for the primer gas interaction, 4) a drag correlation, and 5) a heat-transfer correlation. Drag and heat-transfer data are nonexistent as appropriate input to the problem under study. All of the foregoing semiempirical relations leave the theoretician with so many adjustable parameters that it is possible to duplicate certain experimental data, such as the pressure history at a given location. Not until the pressure and the gas and particle velocity are measured simultaneously at a location, or until the nonsteady ignition flame front is recorded along with the pressure field, can any model be tested properly. It must be noted however, that the modeling efforts are useful in the sense that parametric sensitivity studies can

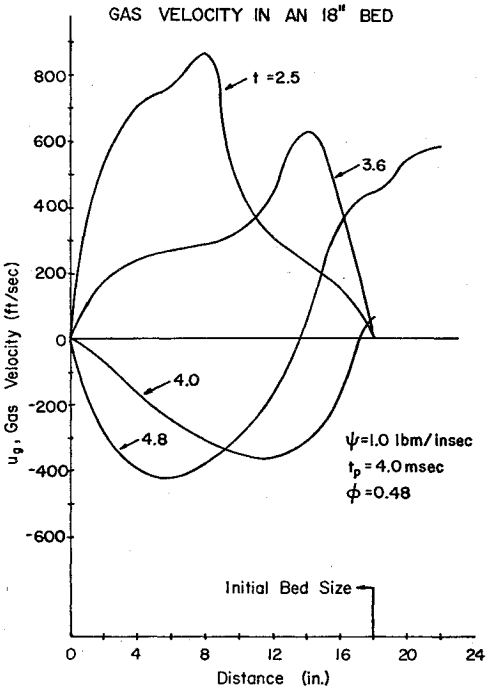

Fig. 7 Gas velocity distribution history predicted for conditions simulating a 76-mm cartridge.

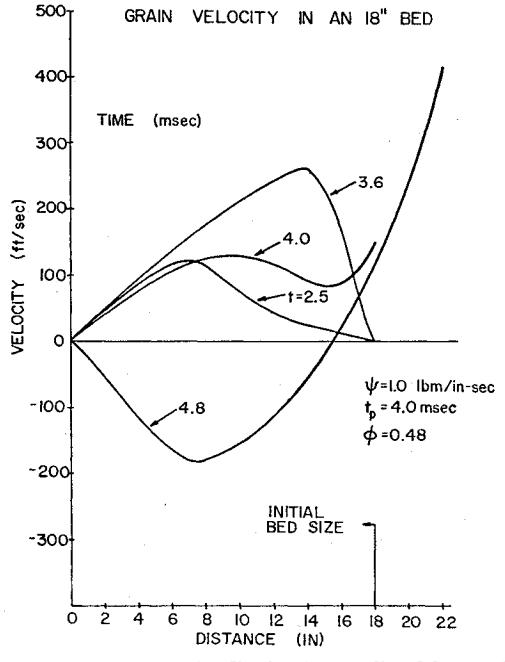

Fig. 8 Propellant grain velocity distribution predicted for conditions simulating a 76-mm cartridge.

be carried out to identify which properties are relatively more important in describing the pressure field.

Concerning the availability of experimental tests with solid-propellant grains in closed tubes, it is evident that a large amount of testing is yet to be carried out in order to confirm the validity of our model and its required constitutive relations. In addition to the Russian work cited by Belyayev and Bobolev[18] with granular explosives, there are experiments by Squire and Devine,[19] by Gerri, et al.,[20] and by Alkidas et al.[21] which deal with packed beds of small spherical solid propellant. With larger multiperforated propellant grains there are reported experiments by Soper,[22] McClure and East,[7] Heddon and Nance,[23] Horst,[24] and Clarke and May.[25]

The general conclusion that can be drawn from a review of these experimental studies are that the type of ignition source (end-on or perforated tube insert) is one of the most important factors that determines the pressure dynamics. The amount of propellant loading (ϕ) and the confinement of the grains is obviously a factor. Other general observations are that the convective driven flame ignites the propellant bed at speeds ranging from 5-20 in./msec (0.125-0.50 mm/μsec), that, in general, the propellant grains are mobile, and that the pressure rises more rapidly as one moves forward from the igniter end. This last observation implies that there exists a "continental divide" (term first used by Kuo *et al.*[2]) or peak pressure in the interior of the bed. It appears that center-core igniters, evenly distributing the ignition source, can smooth out the pressure distribution, minimizing this reverse pressure difference and the subsequent pressure oscillations during the flame-spreading sequence.

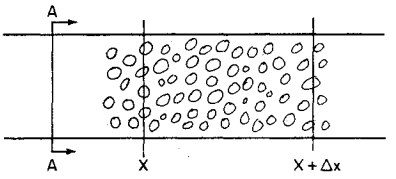

Fig. 9 Control volume to calculate proper pressure gradient force.

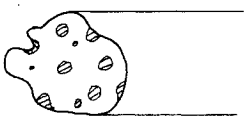

Fig. 10 Cross-section interface $A=A$ from Fig. 9.

Appendix A: Pressure Gradient Force

Consider a control volume, as shown in Fig. 9. Figure 10 shows the cross-section interface, A-A. The cross-hatched regions represent portions of the solid through which the control surface passes.

For the two phases, let A^g be the cross-sectional area of the gas and A^s the area of the solid. The pressure force term can be developed as follows:

$$p^gA^g+p^sA^s-\left[\left[p^g+\frac{\partial p^g}{\partial x}\Delta x\right]\left[A^g+\frac{dA^g}{dx}\Delta x\right]\right]$$

$$-\left[\left[p^s+\frac{\partial p^s}{\partial x}\Delta x\right]\left[A^s+\frac{dA^s}{dx}\Delta x\right]\right]=p^gA^g+p^sA^s$$

$$-\left\{p^gA^g+\left[\frac{\partial p^g}{\partial x}A^g+p^g\frac{\partial A^g}{dx}\right]\Delta x+\text{h.o.t.}-p^sA^s\right.$$

$$\left.+\left[\frac{\partial p^s}{\partial x}A^s+p^s\frac{dA^s}{dx}\right]\Delta x+\text{h.o.t.}\right\}=-\frac{\partial}{\partial x}(p^gA^g)$$

$$-\frac{\partial}{\partial x}(p^sA^s)=-\frac{\partial}{\partial x}\left[p^g\frac{A^g}{A_T}A_T\right]-\frac{\partial}{\partial x}\left[p^s\frac{A^s}{A_T}A_T\right] \tag{A1}$$

where A_T = total cross-sectional area, assumed constant.

In the one-dimensional case, the correspondence between A^g/A_T and ϕ is complete, i.e.,

$$A^g/A_T=A^g\Delta x/A_T\Delta x=V_g/V_T\equiv\phi \tag{A2}$$

and

$$A^s/A_T=A^s\Delta x/A_T\Delta x=V_s/V_T\equiv 1-\phi \tag{A3}$$

Hence, the pressure gradient force can be written as

$$-(\partial/\partial x)\ (\phi p^g)-(\partial/\partial x)\ ([1-\phi]p^s;\quad A_T=\text{const} \tag{A4}$$

In the model,[1] we have taken $p^s \equiv 0$, and then the term

$$-(\partial/\partial x)\ (\phi p^g) \tag{A5}$$

will appear in both the gas species momentum balance and in the mixture equation.

Note the behavior of this term, as $\phi \to 0$ or $\phi \to 1$ is correct; i.e., it gives zero pressure gradient either as $\phi \to 0$ (no gas) or as $\phi \to 1$ (all gas). Notice that, because the ϕ term appears on the inside of the brackets, one must conclude that, for proper static equilibrium at the initial condition $t=0$, when $p^g = \text{const}$ and $U^g = 0$, the gas phase momentum equation also requires $\phi = \text{const}$. That is, the continuum, one-dimensional analysis cannot allow an initial porosity variation in the bed, unless, of course, there exists a corresponding pressure variation for static equilibrium.

An Alternate Approach

Consider the control volume, representing a quasi-one-dimensional two-phase flow as depicted in Fig. 11. Then

$$\phi = A_g \Delta x / S_1 \Delta x = A_g / S_1; \quad \text{and } 1-\phi = A_s/S_1$$

and $S_1 = \text{total inlet area for the mixture} \equiv A_T$. The proper force balance for the total mixture-pressure P_m when accounting for the additional horizontal component of the pressure force acting on the boundary surface of the fluid element is

$$F = P_m S_1 - (P_m + dp_m)\ (S_1 + dS_1) - (P_m + \tfrac{1}{2} dP_m) dS_1 \tag{A6}$$

Thus

$$F = -S_1 dP_m \tag{A7}$$

Thus the pressure gradient term, in this case, is equal to

$$-(A^s + A^g)\ (d/dx)\ (p^g + p^s) \tag{A8}$$

or

$$-S_1[\phi(dP^g/dx)] - S_1(1-\phi)\ (dP^s/dx) \tag{A9}$$

But now assume that the particle pressure $P^s = P^2$. Then

$$-\phi(\partial P^g/\partial x) \tag{A10}$$

represents an alternate form of the pressure gradient in the gas phase momentum balance per unit flow volume, $S_1 - x$

Appendix B: Species Partial Stress Tensor

Consider the mixture to be a perfect fluid

$$\rho(DU_i/dt) = -(\partial P/\partial x_j)\delta_{ij} \tag{B1}$$

where U_i is the mixture velocity and ρ is the mixture density. The fundamental identify is written as

$$\rho \frac{DU_i}{Dt} = \sum_{\alpha=1}^{\Re} \left\{ \rho^\alpha \frac{Du_i^\alpha}{Dt^\alpha} + \mathfrak{u}_i^\alpha \Gamma^\alpha - \frac{\partial}{\partial x_j} [\rho^\alpha \mathfrak{u}_i^\alpha \mathfrak{u}_j^\alpha] \right\} \tag{B2}$$

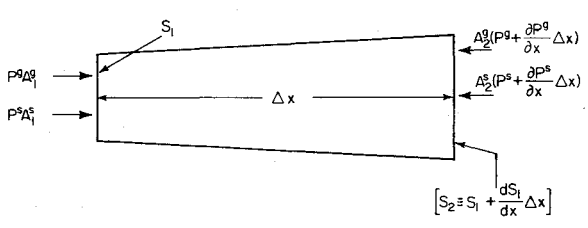

Fig. 11 Control volume of a quasi-one-dimensional two-phase flow.

where $\mathfrak{u}_i^\alpha$ is the diffusion velocity ($\mathfrak{u}_i^\alpha = u_i^\alpha - U_i$). The total pressure is assumed to be the sum of the partial pressures:

$$p = \sum_{\alpha=1}^{\Re} p^\alpha \tag{B3}$$

Putting (B2) and (B3) into (B1) yields

$$\sum \left\{ \rho^\alpha \frac{Du_i^\alpha}{Dt^\alpha} + \mathfrak{u}_i^\alpha \Gamma^\alpha - \frac{\partial}{\partial x_j} [\rho^\alpha \mathfrak{u}_i^\alpha \mathfrak{u}_j^\alpha] \right\} = -\frac{\partial}{\partial x_j} \sum_{\alpha=1}^{\Re} p^\alpha \delta_{ij} \tag{B4}$$

From this, the species momentum balance is deduced to be

$$\rho^\alpha (DU_i^\alpha/Dt^\alpha) = -(\partial P^\alpha/\partial x_j)\delta_{ij} + (\partial/\partial x_j)\ [\rho^\alpha \mathfrak{u}_i^\alpha \mathfrak{u}_j^\alpha] - \mathfrak{u}_i^\alpha \Gamma^\alpha + \hat{p}_i^\alpha \tag{B5}$$

where

$$\sum_{\alpha=1}^{\Re} \hat{P}_i^\alpha \equiv 0$$

The species stress tensor is seen to be

$$\tau_{ij}^\alpha = -P^\alpha \delta_{ij} + \rho^\alpha \mathfrak{u}_i^\alpha \mathfrak{u}_j^\alpha \tag{B6}$$

For one-dimensional nonreacting flow, we get

$$\rho^\alpha [(\partial u^\alpha/\partial t) + u^\alpha (\partial u_\alpha/\partial x)] = -(\partial P^\alpha/\partial x) + (\partial/\partial x)\ (\rho^\alpha \mathfrak{u}^{\alpha 2}) + \hat{P}_x^\alpha \tag{B7}$$

The apparent discrepancy between Eq. (B7) and the species momentum equation as derived by Gough[3] or Kuo et al.[2] for an inviscid fluid can be traced as follows. Let σ_{ij}^α be taken as $-P^\alpha \delta_{ij}$. Hence, different partial stress tensors were assumed. To illustrate the effect of this, we shall derive the resulting mixture equation. For now, we neglect body forces, combustion, etc.; then

$$\rho^\alpha / Du_i^\alpha / Dt^\alpha) = -(\partial P^\alpha/\partial x_i) \tag{B8}$$

is the species momentum balance equation.

From the fundamental identify [Eq. (B2)], we can write

$$\rho \frac{DU_i}{Dt} = \sum_{\alpha=1}^{\Re} \left\{ \rho^\alpha \frac{Du_i^\alpha}{Dt^\alpha} - \frac{\partial}{\partial x_j} (\rho^\alpha \mathfrak{u}_i^\alpha \mathfrak{u}_i^\alpha) \right\} \tag{B9}$$

Substituting (B8) into (B9) yields

$$\rho \frac{DU_i}{Dt} = -\frac{\partial P}{\partial x_j}\delta_{ij} - \sum_{\alpha=1}^{\Re} \frac{\partial}{\partial x_j} (\rho^\alpha \mathfrak{u}_i^\alpha \mathfrak{u}_j^\alpha) \Big\} \tag{B10}$$

If Eq. (B3) still holds, as it should, this can be written as

$$\rho \frac{DU_i}{Dt} = -\frac{\partial P}{\partial x_j}\delta_{ij} - \sum_{\alpha=1}^{\Re} \frac{\partial}{\partial x_j} (\rho^\alpha \mathfrak{u}_i^\alpha \mathfrak{u}_j^\alpha) \tag{B11}$$

Equations (B11) and (B1) are not identical. Note that Eq. (B11) is, however, identical to the mixture momentum equation for an inviscid fluid, as derived by Williams[26] of Appendix C of this text. Equation (B11) does not describe a truly Newtonian fluid, and hence the assumption that $\sigma_{ij}^\alpha = -P^\alpha \delta_{ij}$ violates the basic constitutive assumption of the model used in this paper. The conclusion is that the model derived in Ref. 1is consistent with the stated assumptions. It is not obvious whether Eq. (B1) or (B11) is the absolutely correct mixture equation to use. The constitutive assumptions concerning the mixture, therefore, determine which one to use, and hence whether Eq. (B7) or (B8) is the proper species momentum equation.

References

[1]Krier, H., Van Tassell, W. F., and Rajan, S., "Model of Flame Spreading and Combustion Through Packed Beds of Propellant Grains," BRL-CR-147, March 1974, Ballistic Research Lab.; also Rept. 74-1, 1974 Aeronautical and Astronautical Engineering Dept., University of Illinois at Urbana-Champaign, Urbana, Ill.

[2]Kuo, K., Vichnevetsky, R., and Summerfield, M., "Theory of Flame Front Propagation in Porous Propellant Charges Under Confinement,' *AIAA Journal*, Vol. 2, April 1973, pp. 444-451.

[3]Gough, P. S., "Fundamental Investigation of the Interior Ballistics of Guns," Rept. SRC-R-75, July 1974, Space Research Corporation.

[4]Truesdell, C. and Toupin, R. A., "The Classical Field Theories," *Handbuch der Physik*, edited by S. Flügge, Vol. 3, Pt. 1, Springer-Verlag, Berlin, 1960. [Particular sections of interest are Sec. 158, p. 469: "Kinematics of Diffusion in a Heterogeneous Mixture'; Sec. 159, p. 472: "Conservation of Mass in a Heterogeneous Mixture"; Sec. 215, p. 567: "Partial Stress in a Heterogeneous Mixture"; Sec. 243, p. 612: "Balance of Energy in a Heterogeneous Mixture"; Sec. 254, p. 634: "Heterogeneous Media I. Compatability of an Equation of State for the Mixture with Equation of State for the Constitutents"; Sec. 255, p. 636: "Heterogeneous Media II. Explicit Form of the Gibbs Equation."]

[5]Krier, H. and VerShaw, J. T., "Process of Fluidization During Porous Solid Propellant Combustion," AAE Rept. 74-8, Spet. 1974, Aeronautical and Astronautical Engineering Dept., Univ. of Illinois at Urbana-Champaign, Urbana, Ill.

[6]Rajan, S. "Evaluation of Numerical Viscosity Effects in Transonic Flow Calculations," AIAA Paper 73-131, Washington D.C. 1973.

[7]McClure, D. R. and East, J. L., "Experimental Techniques for Investigating the Start-up Ignition/Combustion Transients in Full-Scale Charge Assemblies," *Proceedings of the 11th JANNAF Combustion Meeting*, CPIA Publ. 261, Dec. 1974, pp. 119-139.

[8]Krier, H., "Predictions of Flamespreading and Pressure Wave Propagation in Propellant Beds," AAE Rept. 75-6, 1975, Aeronautical and Astronautical Engineering Dept., Univ. of Illinois, Urbana, Ill.

[9]Ergun, S., "Fluid Flow Through Packed Columns," *Chemical Engineering Progress*, Vol. 48, 1952, p. 89.

[10]Carman, P. C., "Fluid Flow Through Granular Beds," *Transactions of the Institution of Chemical Engineers*, Vol. 15, 1937, p. 150.

[11]Bird, R., Stewart, W., and Lightfoot, E., *Transport Phenomena*, Wiley, New York, 1960.

[12]Leva, M., "Pressure Drop Through Packed Tubes, Parts I and II," *Chemical Engineering Progress*, Vol. 48, 1952, p. 89.

[13]Denton, W., "The Heat Transfer and Flow Resistance for Fluid Flow Through Randomly Packed Spheres," American Society of Mechanical Engineers, Sept. 1951.

[14]Coppage, J. and London, A., "Heat Transfer and Flow Friction Characteristics of Porous Media," *Chemical Engineering Progress*, Vol. 52, Feb. 1956, p. 57F.

[15]Chang, T. and Wen, C., "Fluid to Particle Heat Transfer in Air Fluidized Beds," *Chemical Engineering Progress Symposium Series*, Vol. 62, 1966. p. 111.

[16]Gelperin, N. and Einstein, V., "Heat Transfer in Fluidized Beds," *Fluidization*, edited by J. Davidson and D. Harrison, Academic Press, London, 1971.

[17]Frantz, J. F., "Design for Fluidization—Part II," *Chemical Engineering*, Vol. 69, Oct. 1962, p. 89.

[18]Belyayev, A. F., Bobolev, V. K., "Transition of the Combustion of Condensed Systems into an Explosion," *Perekhod Goreniya Kondensirovannykh Sistem Vo Vxryv, Izd Vo "Nauka"*, Transl. FTD-MT-0841-75, 1973.

[19]Squire, W. H. and Devine, M. P., "The Interface Between Primer and Propellant," AOA Paper, 1969, Frankford Arsenal, Philadelphia, Pa.

[20]Gerri, N., Pfaff, S. P., and Ortega, A. E., "Gas Flow and Flame Spreading in Porous Beds of Ball Propellant," *Proceedings of the 11th JANAF Combustion Meeting*, Dec. 1974, CPIA Publ. 261, pp. 177-198.

[21]Alkidas, A., Morris, S.O., Caveny, L.H., and Summerfield, M., "An Experimental Study of Pressure Wave Propagation in Granular Propellant Beds," AIAA Paper 75-242, Pasadena, Calif., Jan. 1975.

[22]Soper, W. G., "Grain Velocities During Ignition of Gun Propellant," *Combustion and Flame Journal*, Vol. 24, pp. 199-202; also Soper, W. G., "Ignition Waves in Gun Chambers," *Combustion Flame*, Vol. 20, 1973, pp. 157-162.

[23]Heddon, S. E. and Nance, G. A., "An Experimental Study of Pressure Waves in Gun Chambers," NPG Rept. 1534, 1957, Naval Weapons Lab., Dahlgren, Va.

[24]Horst, A. W., "Solid Propellant Gun Interior Ballistic Modeling—FY1974 Annual Rept," Rept. IHTR-419, 1975, Naval Ordinance Station, Indian Head, Md.

[25]Clark, E. V. and May, I. W., "Subtle Effects of Low Amplitude Pressure Wave Dynamics on the Ballistic Performance of Guns," *Proceedings of the 11th JANAF Combustion Meeting*, Dec. 1974, CPIA Publ. 261, pp. 141-156.

[26]Williams, W. A., *Combustion Theory*, Addison-Wesley, Cambridge, Mass., 1965, Appendix C. pp. 390-403.